

# FOCMEC: FOCal MEChanism Determinations

*J. Arthur Snoke*  
*Virginia Tech, Blacksburg, VA, USA*  
*snoke@vt.edu*

## Abstract

This report accompanies a package of programs for determining and displaying double-couple earthquake focal mechanisms. Input are polarities ( $P$ ,  $SV$ ,  $SH$ ) and/or amplitude ratios ( $SV/P$ ,  $SH/P$ ,  $SV/SH$ ). The main program, *focmec* (coded in Fortran), performs an efficient, systematic search of the focal sphere and reports acceptable solutions based on selection criteria for the number of polarity errors and/or errors in amplitude ratios. The search of the focal sphere is uniform in angle, with selectable step size and bounds. The selection criteria for amplitudes allow correction or weightings for near-nodal solutions. The *FOCMEC* package has been distributed for more than 15 years, and has been cited more than 100 times.

Program *focmec* produces two output files: a complete summary of information about all acceptable solutions, and a summary file that can be used as an input to other programs for further analysis or display. Another program in the package, *focplt*, produces focal-sphere plots based on the *focmec* summary file of input data (polarities and/or ratios) alone or superimposed on solutions (fault planes, compression and tension axes,  $SV$  and  $SH$  nodal surfaces). Program *ratplt* is the ratio plotting program for the *FOCMEC* package. Other auxiliary programs include one to create input files for program *focmec*, a program that converts from among various ways of presenting a double-couple solution, a program that calculates the radiation factors for an input mechanism, and programs for displaying and printing plot files. Instructions and scripts are included for compiling and running the programs, and there are two data sets with scripts and documentation for running the programs. If you are reading this manual but have not downloaded the package, the link to the footer will take you to a screen with both the package and a *readme.txt* file with instructions for getting started.

## 1 Introduction and Overview

Given excellent station coverage for an earthquake in a region for which the Earth (seismic velocity) structure was well determined, and with well recorded, impulsive  $P$ -wave first arrivals, one could get a reliable estimate for the fault-plane solution (focal mechanism) for the event. More typically, the station density is low, the velocity structure is known only approximately, and the polarities of the first arrivals are often ambiguous. For imperfect data, one may need to assume a certain number of errors to find “satisfactory” solutions, and in many cases the solutions are not well constrained. For 3-component data,  $SV$  and  $SH$  polarities may be well enough recorded that they can be used to constrain fault-plane solutions. The range of possible solutions can often be further constrained if one can read, to within 10%, the  $P$  amplitudes on vertical-component seismograms and  $S$  amplitudes on one or more components, and use amplitude ratios.

On the IRIS software server (link in footer below) there are three files: *focmec.tgz* (a compressed tar file containing the *FOCMEC* package), *readme.txt* (a file with instructions to download the package, build the package, and a brief summary of changes since the penultimate version), and *focmec\_manual.pdf* (this file). After downloading and expanding the package file, the top directory is *focmec*, which in turn has several sub-directories.

Instructions for building and testing the package are in HTML format. One starts by opening *./focmec/doc/focmec.html*. Documentation for the package can be accessed by following the links to other HTML files. Also in *./focmec/doc* are subdirectories with the output files from scripts in the *./focmec/sample\_runs/* subdirectories. If you used earlier versions of the package, I encourage you to look at *./focmec/doc/update.html*. Of particular note to those who worked with ratio data are two modifications: (1) a slight change in the input-file format, and (2) runs for the same input data for earlier versions may not give the same answers now. These modifications are discussed in Section 4.2.3.

The first version of program *focmec* was written in 1984 (Snoke *et al.*, 1984). The programs have been built and run on IBM/CMS, PDP/RSX, VAX/VMS, Sunos. Sun Solaris, Windows 98, Linux, and Mac OS X (PPC and i686). The programs are written in Fortran and compile successfully using *gfortran*, *g77*, and Sun's *f77*. A program (*sgftops*) coded in C (*gcc*) transform graphics plot files from the graphics format used by the plotting programs (files ending in.sgf) to postscript. Unix scripts (csh) are included for displaying plots on the screen and for converting plot files from postscript to EPS or PDF. The plot-conversion scripts require the external program *ghostscript*. If the user has or prefers a different EPS or PDF viewer for displaying plots (such as *gv* on Linux), it is easy to modify the plot-display script. Except for these plot-conversion scripts, X-Windows capability is not required by the *FOCMEC* package.

Although the *FOCMEC* package has been cited in more than a hundred publications, the only non-abstract I have published is Snoke (2003). I wrote *focmec* for Virginia Tech professor Gil Bollinger and his students at Virginia Tech because they could not find a good focal-mechanism program to use in their studies of local and regional earthquakes. The *FOCMEC* package has been made available for several years for download from IRIS and has been part of the *SEISAN* earthquake-analysis package (Ottemller, *et al.* 2016). A good overview of the *FOCMEC* package is included in Rau *et al.* (1996), and a recent publication shows how *S* polarities and amplitude ratios can be used to obtain well-constrained focal mechanisms for small events recorded by sparse networks is Wu *et al.* (2015). A useful primer on the use of amplitude ratios in calculating focal mechanisms is included in Julian *et al.* (1906), who use a different method from that used in *focmec* to calculate focal mechanisms. Ebel and Bonjer (1990) discuss potential problems in finding accurate estimates of *P* and *S* amplitudes when studying small, shallow, nearby (10–100 km) earthquakes.

The next section in this report has a discussion of the programming essentials and data preparation. The following section has a description of the programs that make up the package. The final section includes descriptions, input, and output for sample runs. Appendix A contains detailed instructions on how to prepare an input file for program *focmec*. Appendix B contains definitions of terms used when discussing focal mechanisms. Appendix C has cautionary comments for those who want to use *SV* polarities and amplitudes, Appendix D discusses graphics in the context of the *focmec* package, and Appendix E has a description and discussion of the *focmec* grid-search procedure.

## 2 Programming Procedure, and Data Preparation

### 2.1 Programming Procedure for *focmec*

The data (station identifiers, azimuths, take-off angles at the source, polarities, and/or amplitude ratios from among *P*, *SV*, and *SH* arrivals) are read in from a text file. Selection parameters are entered through run-time prompts, or from user-customized script files. Depending on the input data, prompts include the number of allowed polarity errors, an acceptable range for deviations between the observed and calculated amplitude ratios, the maximum number of allowed ratio errors, the region of the focal sphere to be searched, and the fineness/coarseness of the search. (If there are no ratio data, there are no prompts related to ratios, so the same script cannot be used for a file with ratios data and a file with no ratios data.) Using these search criteria, program *focmec* systematically tests all possible focal mechanisms and lists those consistent with the selection criteria.

All acceptable focal mechanisms are stored in two files: a short file (default: *focmec.out*) with one line per solution that can later be used as an input file for a plotting program, such as *focplt*, and a more complete listing file (default: *focmec.lst*) that includes four representations of the solutions (dip, strike, rake for either possible fault plane; the **A** and **N** axes trends and plunges, the **P** and **T** trends and plunges; and the moment tensor), the station identifiers for those with a polarity error, and complete information on the calculated and theoretical amplitude ratios for each input ratio. The conventions used are as in *Aki and Richards* (2002, pp. 101–113) and *Herrmann* (1975), except that our **A** and **N** axes correspond to Herrmann’s **X** and **Y** axes. (See Snoke (1989) or Herrmann (1975) for a review of the terminology and conventions related to focal mechanism determinations.)

Two sets of input parameters deserve special mention: for polarities, relative weighting; and for ratios, *P* and *S* radiation-factor “cut-offs”.

1. The traditional polarity weighting is to assign an error measure of “1” for every calculated polarity that does not match the observed polarity. (Henceforth, I will refer to this approach as UW for *unity weighting*.) An option in the program is to use *relatively-weighted* (RW) polarity errors; a mismatch for data near a nodal surface counts less than a mismatch near the middle of the quadrant. (See Figure B3.) The weight for a polarity using RW is the calculated absolute value of the calculated radiation factor, so the range is 0.0 to 1.0. Hence allowing for 0.2 RW in a *focmec* run might include near-nodal-plane errors at more than one station. Starting in 2017, the default is RW, as I think RW better reflects the polarity error than UW does.

Program *focmec* does not code the quality of arrivals. It does, however, include a separate coding for *emergent arrivals*, and a run-time *focmec* option is to include or leave out emergent-arrival picks in the polarity data. Hence, one can code lower-quality arrivals as *emergent* and compare results from runs with and without emergent-arrival picks.

2. For an amplitude ratio, if the numerator or denominator calculated radiation factor is near a nodal surface, the result is a large absolute value for the calculated  $\log_{10}(\text{ratio})$ .

Threshold factors for  $P$  and  $S$  are chosen (default 0.1 for both numerator and denominator). If the radiation factor for either the numerator or denominator phase is less than the chosen cut-off, that factor gets replaced by the cut-off value when calculating the ratio. Flags in the complete-solution output file (default name *focmec.lst*) indicate cases in which the numerator (flag NUM) or denominator (flag DEN) is below the cut-off to let the user know that those ratios may have to be examined more closely. If both the numerator and denominator radiation factors are below the cut-offs (flag N&D), that ratio is indeterminate.<sup>1</sup>

Both of these follow, in part, from the assumption that because the event location and/or the velocity structure may not be well constrained, polarity errors or amplitudes near a nodal surface should not have the same weight as those further from a nodal surface.

## 2.2 Data Preparation

The polarity conventions and the notation for amplitude ratios are included in Appendix A. My procedure for calculating amplitudes and amplitude ratios is discussed in Section 4.2.1.

Before using  $SV$  data, read Appendix C because if the  $S$ -emergence angle is beyond the

## 3 Programs in addition to *focmec*

### 3.1 Additional Analysis Programs

Three subsidiary analysis programs are included: *dsretc*., *radiat*, and *freesurf*. Source (.f) files are in *./focmec/src/*. The programs are self-contained, and they can be run from scripts.

- Program *dsretc* allows one to convert from among the various ways to represent a focal mechanism. Input options are one from among three representations of a focal mechanism: dip, strike, rake; plunge/trend for **P** and **T**; the moment tensor (which is not restricted to a double-couple solution). Output includes all representations plus angles that can be used to fine-tune the *focmec* grid search to a single mechanism (see Appendix E).
- Program *radiat* produces radiation factors and amplitude ratios for input dip, strike, rake, take-off angle, and azimuth. These factors are used if RW is chosen for polarity errors.
- Program *freesurf* calculates free-surface corrections that are useful when preparing ratio input to *focmec*. See Figure C2.

### 3.2 Plotting Programs

- Program *focplt* is the main plotting program in the *FOCMEC* package. Input can be from the *focmec* input file (for polarity data) and/or from the *XXX.out* output file (for one or more solutions) and/or dip, strike, rake for single solutions. The plots are equal-area Lambert-Schmidt projections (default lower hemisphere) of the focal sphere. Plots can include any or all from among the following: polarity data and/or fault planes, *SV* or *SH* nodal surfaces, or **P**, **T**, **B** axes. There are options for adding time stamps, a title, and labels. The program can be run from scripts or interactively from the terminal. Sample scripts are included in *./focmec/sample\_runs/*.
- Program *ratplt* is the ratio plotting program for the *FOCMEC* package. One is prompted for a *focmec* input file from which it selects all ratio data. Next one is prompted for the dip, strike, and rake for a focal mechanism and *a*, the maximum allowed absolute value of the difference between the  $\log_{10}$  observed-minus-calculated ratios for that focal mechanism (*a*). Finally, one is prompted for a plotting scale factor *s*. Defining *d* as the absolute value of the difference for each ratio, the output is a focal-sphere plot of the  $s10^d$  for each ratio (keyed to the type of ratio) superimposed on the  $s10^a$ . Output for *ratplt* are shown in Figure 4 below, and the driver script are in *./focmec/sample\_runs/sakhalin*.
- Programs and scripts are included that allow one to display output plot files on the screen as well as to convert plot files to Postscript, EPS, and PDF. Further information on these programs and scripts is included in Appendix D.

### 3.3 Traveltime Tables

For the example discussed in Section 4.2, take-off angles and traveltimes are calculated using *iaspei-tau* traveltime tables. (Traveltimes are needed if one wants to do a Q correction for amplitudes.) Software for producing such tables is included in this package. Tables are calculated for three models: *ak135* (Kennett *et al.* 1995), *iasp91* (Kennett *et al.* 1991), and the *nocrust* model that is *ak135* but with no crust. The traveltime tables are built and placed in directory `./focmec/lib/`. Files with ASCII representations of the two models are in directory `./focmec/iaspei-tau/build-tables`. Program *ttimes* is effectively a mini-tutorial on using the traveltime tables, and `./focmec/tests/run_ttimes` is a script that does a run for that program. Program *ttimes* is used in the analysis of the Sakhalin Island event (Section 4.2) to check the relative arrival times of *S* and *SKS*. For more information about the *iaspei-tau* package, see Snoke (2009) and/or go to URL <http://www.iris.edu/pub/programs/iaspei-tau/>.

Programs *ratio-prep* uses traveltime tables along with the polarity and ratio data to prepare a *focmec-prep* input file. Program *ratio-prep\_1layer* was written in 2017 as an alternative to *ratio-prep* for a data set of shallow-earthquake aftershocks that are recorded at epicentral distances less than 20 km for which the velocity model has a single layer with a layer-thickness greater than the focal depths of the events. For such a geometry, all rays travel upwards within that layer, so raypaths can be calculated using plane geometry. The program takes into account the station elevation, assuming the velocity between sea level and the station is the same as that in the layer. If such a program is of interest to you, see the comment lines at the beginning of `./focmec/src/ratio-prep_1layer` for instructions to prepare input files.

## 4 Applications

Directory `./focmec/sample-runs` has two subdirectories:

1. In Section 4.1 (`./focmec/sample-runs/ETNEvent`) I discuss how one can use the *FOCMEC* package to find the “best” focal mechanism from a data set of *P*-wave polarities collected from stations at local-to-regional distances for a small crustal-depth earthquake.
2. In Section 4.2 (`./focmec/sample-runs/sakhalin`) I show how a sparse data set that includes *S* polarities and amplitude-ratio data can provide a perhaps surprisingly good focal mechanism.

### 4.1 A data set of *P*-wave polarities

Directory `./focmec/sample-runs/ETNEvent` includes drivers, and input files for an application of the *FOCMEC* package to find the focal mechanism for a magnitude 4.2 event using *P* waves recorded by 58 stations at local-to-regional distances on short-period, vertical-component seismographs. The direct *P* waves at 37 stations were well-enough recorded to allow polarity picks. This event, which has a focal depth of 19 km, occurred on 27 March 1987 and is event number 12 in Chapman *et al.* (1997).

The azimuths, take-off angles and picked polarities for the observed *P* waves are in the `.arc` output file from the earthquake-location program *hypoellipse* (Lahr, 1999). The *focmec*

input file was created using program *hypo2foc* that gets its input from the *.arc* file. Chapman (personal communication) gave me their *.arc* file for this event.

The Chapman *et al.* study used *focmec* exclusively with the UW option for polarity errors. There are no solutions with fewer than four UW errors, and the *focmec* run with a maximum of 4 UW errors has 13 solutions with very little spread. Their chosen mechanism was the one with the median nodal-plane strike.

16 of the 37 stations with assigned polarities are labeled as emergent. At the time they did their study, the programs did not allow one to choose to include or exclude arrivals that were coded as emergent. Now that is an option. Three of the polarity errors are at stations with polarities labeled as emergent. Leaving out all the emergent arrivals and allowing one unity-weighted polarity error leads to 168 solutions with a large spread. For the remainder of this report, emergent arrivals are included in all runs.

Using the RW option produces 168 solutions with a large spread in the fault planes for a cut-off of  $\leq 2.0$  RW errors. The 13 solutions with four UW errors are included, and the RW error for the published solution is 1.97. Running *focmec* with a RW cut-off of 1.75 produces four solutions that have considerable overlap with the 13 solutions with four UW polarity errors. Among those four solutions, two have errors at six stations and two have errors at eight stations. Solutions with four UW-polarity errors and those with a 1.75 cut-off for RW errors are shown in Figure 1a. Shown in Figure 1b is the published solution and the RW solution with the lowest RW error (1.69) superimposed on the data.

I suggest one should always compare solution sets using both methods. For this case, the difference is not significant between using unity weighting and relative weighting.

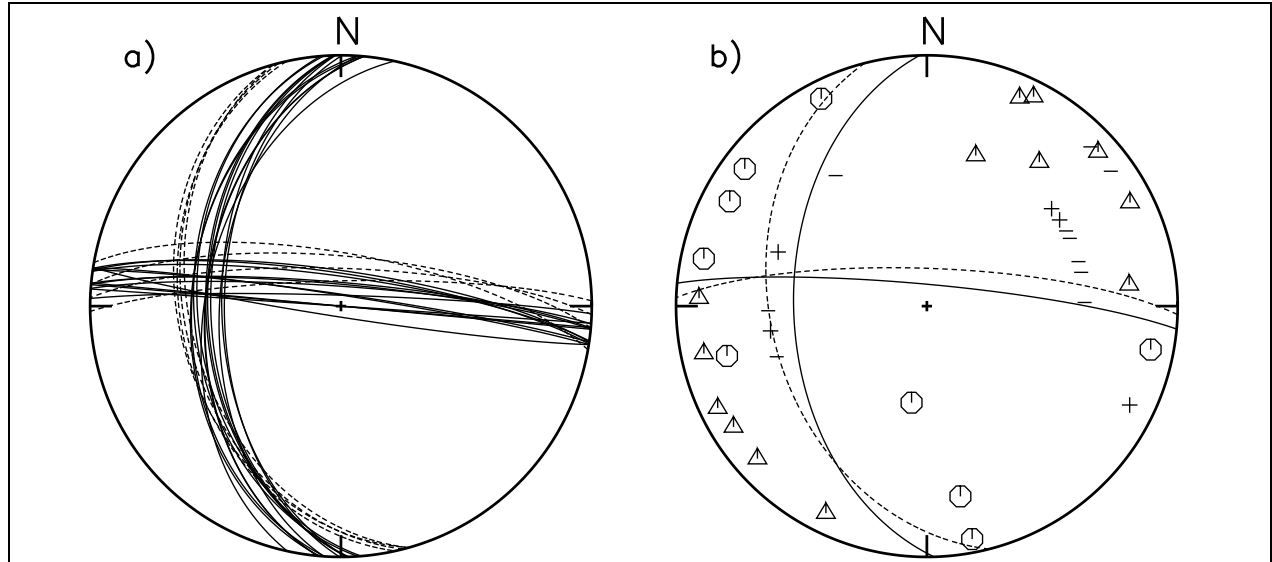


**Figure 1:** Lower-hemisphere projections of the focal sphere from *focplt* runs for Chapman *et al.* (1997) event 12. **(a):** Shown are fault planes of all solutions with four UW-polarity errors (solid lines) and those with a 1.75 RW cut-off (dashes). **(b):** The fault planes for the published focal mechanism (solid line) and the best RW solution (dashes) superimposed on the polarity data. Circles represent compressions and triangles represent dilatations. “+” and “-” indicate emergent compressions and dilatations respectively.

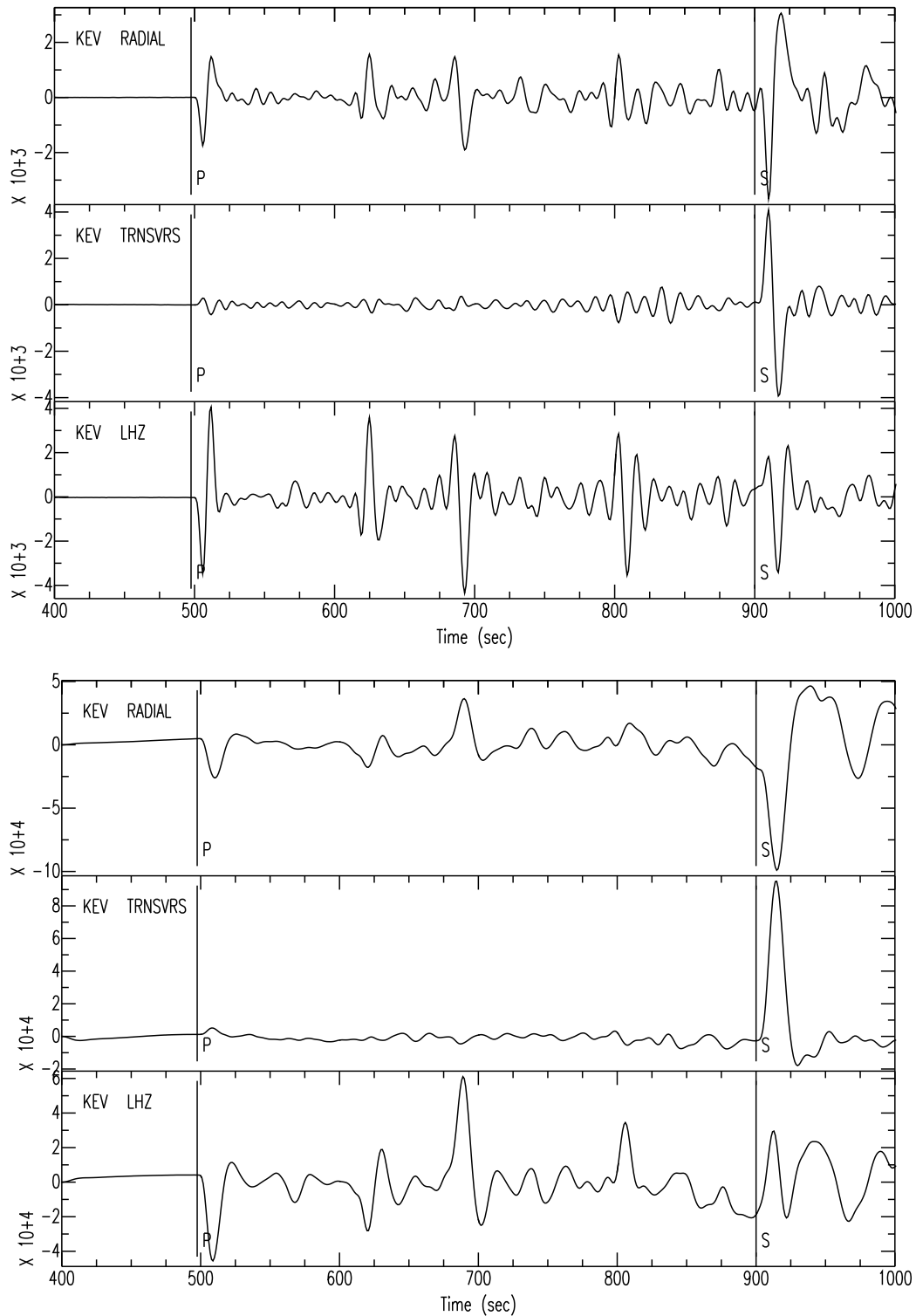


**Figure 2:** Shown are the radial, transverse, and vertical component recordings at KEV for the Sakhalin Island earthquake. **Upper Panel:** Raw recordings (sampled at 1 sps). **Lower Panel:** Instrument-correct and low-pass-filtered (corner 0.05 Hz, 3-pole). Arrival times, calculated using program *ttimes* for the *ak135* model, are marked for *P* and *S*.



## 4.2 Adding *S*-wave polarities and ratios: the Sakhalin Island event

My abstract at the 1990 Eastern Section SSA meeting (Snoke (1990)<sup>2</sup> summarizes my analysis of two methods using very different kinds of data sets that were both available in near-real-time to calculate the focal mechanism for the Sakhalin Island earthquake ( $Z = 611$  km,  $M = 6.5$ , May 12, 1990):

1. a focal mechanism determined from eight broadband stations using *P* and *S* polarities along with amplitude ratios , and
2. a focal mechanism determined using 199 *P*-wave polarities used to produce the preliminary QED/NEIC focal mechanism.

Seven of the eight broadband stations used in the first data set were made available within several hours by IRIS through their newly-developed *GOPHER* system (Malone (1990)), and the eighth was from a newly installed station at BLA (Blacksburg, VA), my home institution.

For this *FOCMEC* manual update, I concentrate on how a sparse data set that includes *S* polarities and amplitude-ratio data can provide a perhaps surprisingly good solution. Refinements in my analysis procedures as described in this section result in better constrained solutions than those I produced in 1990 — especially in how one calculates and analyzes amplitude ratios. I also show how the *FOCMEC* package can be used to find focal mechanisms using two data sets for the same event. Directory `./focmec/sample_runs/sakhalin/` includes drivers and input files for these analyses.

### 4.2.1 Amplitude-ratio calculations: filtering, free-surface effects and *Q*

For *P* and *S* arrivals to be used in an amplitude ratio, implicit assumptions are that the source process is simple and the phases have effectively the same travel paths. The procedure used by Julian *et al.* (1996) is as follows:

If the frequency content is essentially the same, if the *P* and *S* phases first half cycles have similar rise times, and if the seismometers on which they are recorded are matched, one can in principle calculate the amplitudes from the onsets to the first peaks — perhaps after low-pass filtering to clean up the signals.

The procedure I used for this event is to integrate the waveforms to displacement, low-pass filter the displacement waveforms so that the frequency-content for the *P* and *S* waveforms are similar, and do a differential-*Q* correction for the two phases used in the amplitude ratio. For local and regional events, one rarely sees observed displacement waveforms with displacements of the quality seen in Figure 2. Wu & Chapman (2015) use a procedure that combines the two procedures. Their waveforms are flat to velocity above 1 Hz, and they integrate the waveforms — effectively giving displacements. They then use the first half cycle as the amplitude.

Shown in Figure 2 are the three components (radial, transverse, vertical) at station KEV (epicentral distance 5,825 km). Shown are the raw time series (upper panel) and those arrivals

---

<sup>2</sup>.`./focmec/doc/snoke-esssa90.pdf`

corrected to displacement and filtered (lower panel). The arrivals are remarkably sharp, and the displacement arrivals are well-approximated by single-sided pulses, the “textbook” shape for the far-field displacement of the direct  $P$  or  $S$  body waves.<sup>3</sup>

As discussed in Appendix C, the free surface affects direct  $P$  and  $S$  arrivals, so to compare observed and calculated  $S/P$  amplitude ratios one must include free-surface corrections. For incident  $SH$ , the observed amplitude is twice the actual amplitude for all incident angles. As seen in Figure C2, for incident  $P$  and  $SV$  there is a strong dependence on incident angle. As the pulse width of the arrivals increase, the arrivals average over an increasingly larger depth range. For all  $S/P$  ratios, I used the processed waveforms such as those shown in the lower panel of Figure 2, which have pulse widths of more than 10 s. The *ak135* velocity model used in analyzing the Sakhalin Island event has a two-layer crust with layer thicknesses of 20 km and 15 km, so the arrivals used effectively average over the whole crust. The pulse width is From Figure 2, one sees that the pulse widths are about three times as wide for the processed records as for the raw records. I did runs with the straight *ak135* model and the same model with no crust — the top 35 km had the same velocities as the mantle values just below the Moho. The difference in the calculated amplitude ratios is less than 5% and the “best” solution is not changed, but I get slightly smaller ratio errors for runs using the “nocrust” model. I chose to use the “nocrust” model for this study.<sup>4</sup>

For a displacement waveform, the  $Q$  correction is done in the frequency domain. If  $A(\nu)$  is the amplitude at frequency  $\nu$ , the correction is

$$A(\nu) \Rightarrow A(\nu)e^{(-\pi\nu T/Q)} \equiv A(\nu)C(\nu, T/Q), \quad (1)$$

where  $T$  is the traveltime and  $Q$  the (assumed frequency independent) average anelasticity. (See, for example, Rau *et al.* (1996).) The traveltime is longer and  $Q$  smaller for  $S$  compared to  $P$ , so if there is no  $Q$ -correction, the observed  $S/P$  ratio will be smaller than the theoretical ratio that assumes an infinite  $Q$ .

The *FOCMEC* package does not work directly with waveforms; it uses  $T/Q$  for the arrivals to calculate an amplitude correction for each  $S/P$  amplitude ratio. The  $Q$ -correction factor used in program *focmec\_prep* is  $C(\nu_c, T_P/Q_P)/C(\nu_c, T_S/Q_S)$ , where  $\nu_c$  is a “characteristic” frequency representative of the  $P$ -wave displacement pulse. To estimate  $\nu_c$  for the Sakhalin-Island-event data set, I started with a one-sided pulse with a duration of about 10 s, did an FFT, multiplied the frequency-domain signal by  $C(\nu, T/Q)$  using values of  $T/Q$  at the farthest station (TOL). After transforming back to the time domain, I low-pass-filtered the output signal (Butterworth, 3 pole, corner 0.05 Hz) and saved the result, which I define to be  $U(t, T/Q)$ . I did this procedure twice: first with  $T/Q = 2.6$  for  $S$  and then  $T/Q = 0.7$  for  $P$ .  $R$  is defined as the ratio of the maximum of  $U(t, T_P/Q_P)$  to the maximum of  $U(t, T_S/Q_S)$ . Then,

$$\nu_c = \frac{R}{\pi [T_S/Q_S - T_P/Q_P]}. \quad (2)$$

<sup>3</sup>For more about the seismograms at KEV, look at [./focmec/doc/sakhalin-doc/KEV\\_phases.pdf](#)

<sup>4</sup>A 5% error is small, but I include the previous discussion because the differences will be much larger if the velocity model had a thin sedimentary layer at the surface for the analysis of a teleseism or even a regionally-recorded earthquake.

For the Sakhalin Island event, I get  $\nu_c = 0.03$ . This number is in the input data file for each ratio and is used by program *focmec\_prep*.

When there are ratio data in the input file, program *focmec* prompts for the maximum allowed number (N) of ratio errors (defined as the absolute value of the observed-minus-calculated  $\log_{10}$  of the ratios after correcting for the free-surface and Q) and a cut-off (a chosen maximum value of the ratio error). For each solution that meets the specified criteria, the output file gives the number of ratios for which there is no ratio error greater than the cut-off, the RMS errors of those acceptable ratios, and the absolute value of the maximum difference of the acceptable ratios.

#### 4.2.2 Analysis of the broadband data

From the eight three-component stations, there are at most 24 polarities and 16 (independent) amplitude ratios. At the four stations with the largest epicentral distances, phase *SKS* comes in from 0s to 17.8s before direct *S* and is visible on the vertical- and radial-component seismograms.<sup>5</sup> Because the *SKS* – *S* time is zero at station CCM, *SV* is not used at all for that station. At two of the three furthest stations, the polarity for *SV* on the radial is clear, but because of visible interference on the radial for the low-pass-filtered displacement waveforms, I considered using *SV/SH* from the raw records.

For station KEV (see Figure 2), I used *SV/SH* from the raw records because of the shape of the *SV* arrival on the filtered radial displacement. The following pulse shapes were not up to my standards, so I did not use them in ratios: *SH* at CCM and *SV* at COR, PAS, and BLA. I ended up with a total of 11 ratios.<sup>6</sup>

My first run was for zero polarity errors and no amplitude-ratio data; the result is 184 acceptable solutions, and the nodal planes very widely (Figure 3a). I then added the ratio data. For zero polarity error and zero ratio errors greater than cut-offs of 0.4, 0.3, 0.2, and 0.16, I found 37, 18, 3, and 1 acceptable solutions respectively. Adding an allowed RW polarity error of 0.2 and one ratio error with the 0.16 cutoff gives three additional solutions — all with zero polarity errors.

**Table 1: Best Solutions for the 8-Station Data Set**

#	Dip	Strike	Rake	AccR/TotR	RMSRErr	AbsMaxDiff	RMS (all)
<b>5-degree spacing</b>							
1.	76.43	59.08	-64.23	11/11	0.0852	0.1543	
2.	77.05	54.08	-59.13	10/11	0.0545	0.1088	0.0999
3.	77.05	59.89	-59.13	10/11	0.0870	0.1325	0.1065
4.	77.76	54.50	-54.06	10/11	0.0880	0.1340	0.1253
<b>1-degree spacing</b>							
5.	79.05	62.39	-65.53	11/11	0.0857	0.1215	
6.	79.14	62.56	-64.51	11/11	0.0871	0.1219	

<sup>5</sup>The *SKS* and *S* traveltimes are calculated using `./focmec/sample_runs/sakhalin/rttimes`.

<sup>6</sup>My procedures and standards have evolved since 2002, when I used all 16 ratios.

“RMSRErr” is the RMS for the acceptable ratio errors, “AbsMaxDiff” is the maximum absolute value of the observed-calculated difference among the acceptable solutions, and “RMS (all)” is the RMS error for all 11 ratios. For the three solutions with one error, the AbsDiff for the ratio that had an absolute value greater than 0.16 are 0.28, 0.22, and 0.31 for #2, #3, and #4. There are no significant differences among the four solutions, which means that the zero-ratio-error solutions are stable.

The grid search used the default  $5^\circ$  for the three angles. I did a set of runs with  $1^\circ$  spacing. For the same search conditions, I found more than 500 solutions. Allowing for zero ratio errors (and zero polarity errors), there are 62, 30, 8, and 2 for ratio-error cut-offs of 0.16, 0.15, 0.14, and 0.13 respectively. The two solutions for a 0.13 cut-off are included in Table 1. The two solutions are almost identical, an expected result when one uses smaller increments in the grid search. Neither of these are significantly better than #1. Solutions #1, #2, and #5 are included in Figures 3b–3d. Hence, I feel that nothing is gained by using the smaller increments, so I will stick with a  $5^\circ$  spacing for my remaining runs and stay with solution #1.

The large number of acceptable fault-plane solutions with no ratio data (Figure 3a) is to be expected from the poor focal-sphere distribution of the eight stations. Adding high-quality ratio data provides a well-constrained solution.

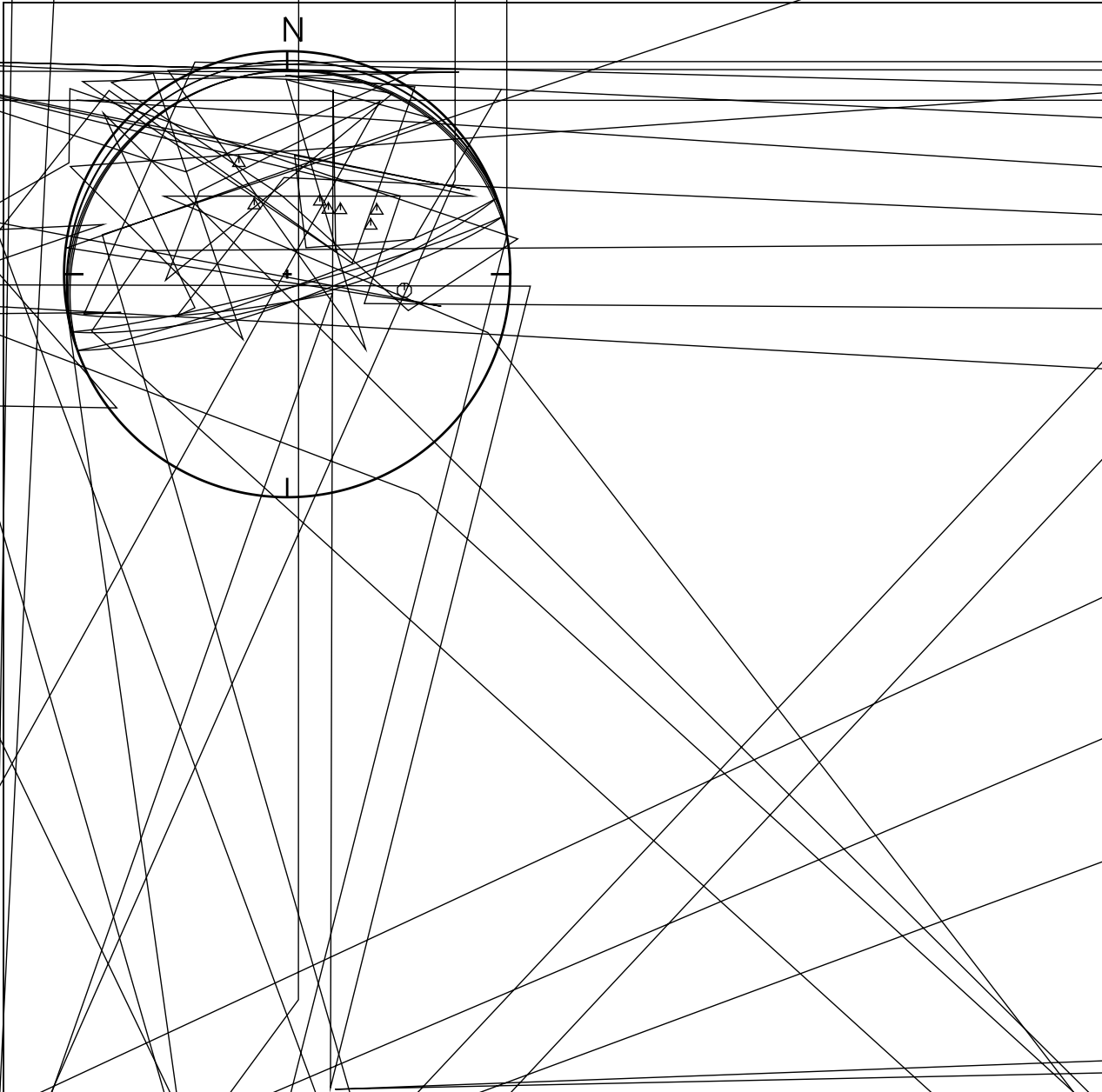
#### 4.2.3 Implications of a modifications for processing ratio data

In December 2013 I modified the procedure for processing  $S/P$  amplitude ratio data, so runs made now with the same data sets as used for the earlier versions of *focmec* may have slightly different answers.

Prior to 2013, I employed the same procedure as that used by Kisslinger and coauthors (1980, 1981, 1982) of using the same take-off angle for both the  $S$  and the  $P$ . If the Poisson’s ratio is constant for the velocities along the raypaths, the take-off angles are the same. Otherwise they are the same. Although I had used both angles in program *focmec\_prep* when processing the observed amplitudes several years earlier, it was not until December 2013 that I used both angles in program *focmec* when calculated the theoretical amplitudes.

I discuss the implications of this modification on solutions created using previous versions of *focmec* in the Web page [./focmec/doc/2013\\_code\\_change.html](http://www.iris.edu/doc/2013_code_change.html). For the example considered, the modification results in changes in solutions that are non-zero, but not significant.

A further modification is a slight change in the input file format for ratio data. If there were ratio data, an earlier versions of the *FOCMEC* package, the  $P$ -to- $S$  velocity ratio at the source (VPVS) was prompted for by *focmec* during a run. Now it is read in from the input file was not prompted for. The change has been made because for a double-couple mechanism,  $(v_P/v_S)^3$  at the source is used to calculate the theoretical amplitude ratio so must be used in preparing the *focmec* input file. Also, I have seen several input files for *focmec* in which one just keeps the default for VPVS which is not correct. Input files written to run for pre-2017 versions of *focmec* need to run program *convert\_input* for each older input file. That program prompts for VPVS.

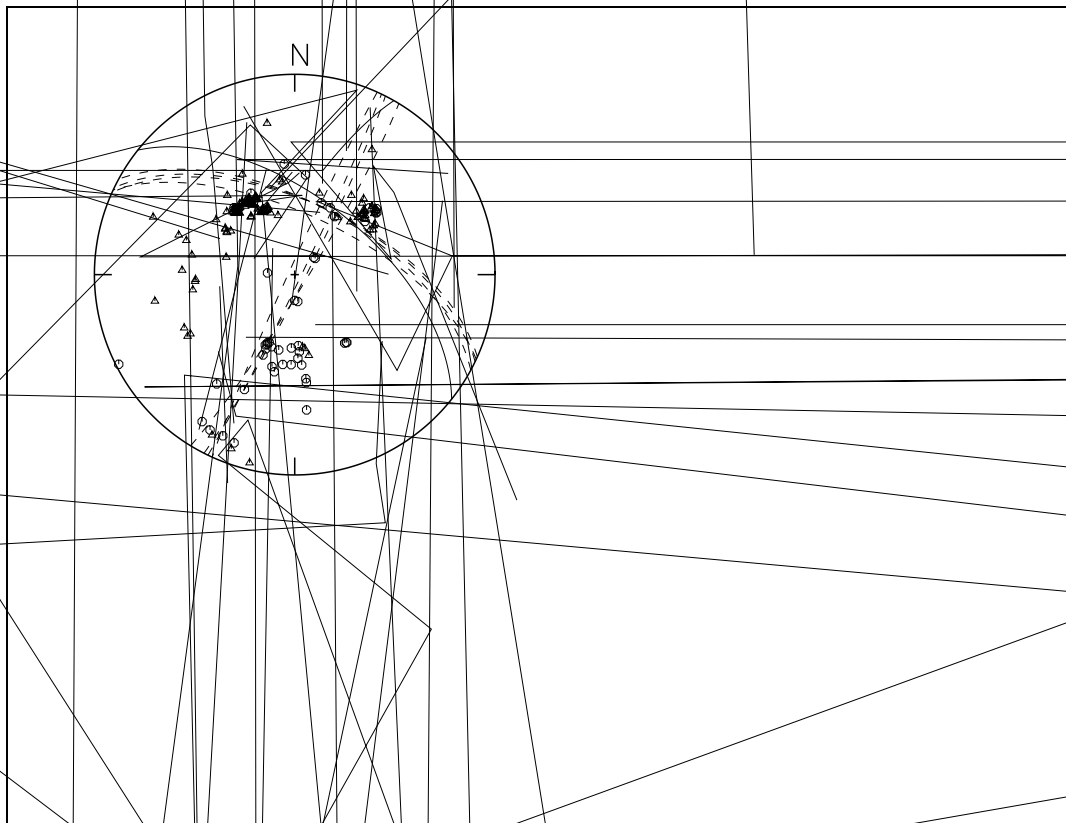


the May 1990 preliminary NEIC QED solution

There are 199 *P*-wave polarities in the preliminary NEIC QED data set, of which nine are labeled as emergent. If I allow 21 UW errors with no emergent arrivals or 22 including emergent arrivals, I get the same five solutions, four with the allowed maximum number and one with one fewer error. The published QED solution is not among these five, although it does not differ significantly (Figure 4a). Restricting the *focmec* grid search to give only the published solution, I get 22 and 21 UW errors with and without emergent stations respectively, with errors at the same stations as for my free runs. For the remainder of this discussion, I will exclude the emergent-arrival stations, so the QED/NEIC data set now has 190 *P*-wave polarity picks.

I assume that both the fact I do not get the QED solution in my free run and that my free run gives a solution with one fewer UW error than the published solution can be explained by the grid search used by NEIC is not the same as used in *focmec* and probably has a coarser spacing.

Figure 4a has focal planes for the five lowest UW-polarity-error solutions and the four smallest RW-polarity-error solutions (cut-off 6.4). There is no overlap for the two solution sets, and there are 124 RW-error solutions with RW less than the published solution value of 6.86.<sup>7</sup> This lack of overlap between best RW and UW solutions is different from the result for the ETN earthquake (Section 4.1) for which the best UW and RW solutions did not differ significantly (Figure 1b). I consider the lack of overlap between UW and RW solutions a potential red flag regarding the quality of the QED data set.



#### 4.2.5 Composite solutions using two data sets from the same event

I combined the two *focmec* input data files. The *P* polarity for station TOL is in both data sets, so the total number of *P* polarities (excluding emergent arrivals) is  $190 + 8 - 1 = 197$ . For the composite data set, I did runs with RW polarity errors. I am confident that the *S* polarity picks are accurate but I specify a 0.2 error in either *SV* or *SH* polarities to allow for the effect of location and/or velocity-model errors on near-nodal-surface solutions. I assumed zero ratio errors and a cut-off of 0.2. I found three solutions. None of them had any *S*-polarity errors, and all the *P*-polarity errors are from the QED data set. In Table 2, the total number of *P* polarity errors is in parentheses. Also included in the table are the *focmec* statistics for the final CMT and 1990 NEIC/QED solutions.

**Table 2: Best Solutions Using the Combined Data Set**

#	Dip	Strike	Rake	P	RMS RErr	AbsMaxDiff
<b>Free run</b>						
1.	<b>80.61</b>	<b>66.98</b>	<b>-69.72</b>	<b>14.7(25)</b>	<b>0.115</b>	<b>0.1989</b>
2.	<b>76.43</b>	<b>59.08</b>	<b>-64.23</b>	<b>14.5(29)</b>	<b>0.085</b>	<b>0.1543</b>
3.	<b>80.95</b>	<b>62.42</b>	<b>-64.66</b>	<b>14.0(26)</b>	<b>0.102</b>	<b>0.1950</b>
<b>Final CMT</b>						
4.	<b>76.17</b>	<b>55.86</b>	<b>-64.11</b>	<b>14.2(29)</b>	<b>0.092</b>	<b>0.1831</b>
<b>1990 NEIC/QED</b>						
5.	<b>78.81</b>	<b>217.07</b>	<b>148.41</b>	<b>6.89(24)</b>	<b>0.490</b>	<b>0.7079</b>

For the NEIC/QED solution, four stations with ratio data were near nodal surfaces for both the numerator and denominator phase, so only seven ratios were considered. For that run, the ratio-error cut-off is 0.9 and there were five acceptable ratios. There are *SH* and *SV* polarity errors: using the convention for *P* errors in Table 2, *SH* has 0.99(7) and *SV* has 1.28(3).

Although the differences for the three free runs are not significant, one would still like to designate one as the “best” solution. To rank solutions #1–#3 in Table 2, one must decide how to evaluate the different kinds of errors: polarity and ratio. Regarding polarity errors, as I have said above, I think RW is better than UW, so the fact that #1 has the lowest number of *P*-polarity errors does not make up for the fact that it has the highest RW. It also has the highest ratio error, so I rejected it. Solution #2 (the best solution for the broadband-station runs) has a lower ratio error but a slightly higher RW polarity error compared to solution #3. Polarity data are in principle more robust than ratio data, but because the QED data set has errors for more than 10% of their *P* picks, I choose the one with the lower ratio error. Hence, #2 is my choice for the “best” solution.

Figures 5a and 5b are *ratplt* plots showing the goodness-of-fit of the log-amplitude-ratio errors for my preferred free-run solution using all the data (5a) and the 1990 NEIC/QED solution (5b). The hourglass height is the same for both sub-figures: 0.16, the lowest value for which the best broadband-station solution has no ratio errors. For 0.16, none of the QED solution is below the cut-off.

File *./focmec/doc/sakhalin-doc/CMT\_solution.pdf* (posted on the Web in 2006), which uses full-waveform inversion, has what I consider the “final” solution for the Sakhalin Island earthquake.<sup>8</sup> As discussed in Appendix E, I used program *dsretc* to find the angles that allow one to restrict the *focmec* grid search to the exact CMT solution. For that solution, there are no polarity or ratio errors, and the RMS log-amplitude-ratio error for the 11 ratios is 0.0916 — effectively the same as my best broadband-station solution.<sup>9</sup> (See Figure 4b.)

---



- Dreger, D. S., H. Tkalčić, M. Johnston (2000). Dilational processes accompanying earthquakes in the Long Valley Caldera, *Science*, **288**, 122–125.
- Dziewonski, A. M., T. A. Chou, and J. H. Woodhouse (1981). Determination of earthquake source parameters from waveform data for studies of regional and global seismicity, *J. Geophys. Res.*, **86**, 2825–2852.
- Ebel, J.E. and Bonjer, K.-P. (1990). Moment tensor inversion of small earthquakes in southwestern Germany for the fault plane solution, *Geophysical Journal International*, **101**, 133–146.
- Goldstein, P., D. Dodge, M. Firpo, and S. Ruppert (1998), What's new in SAC2000? Enhanced Processing and Database Access, *Seism. Res. Letters*, **69**, 202–204
- Gubbins, D. (1990). **Seismology and Plate Tectonics**, Cambridge University Press, Cambridge
- Herrmann, R. B. (1975). A student's guide for the use of  $P$  and  $S$  wave data for focal mechanism determination, *Earthquake Notes*, **46/4**, 29–39,  
URL **<http://srl.geoscienceworld.org/content/46/4/29.full.pdf>**.
- James, D. E. and J. A. Snoke (1994). Structure and tectonics in the region of flat subduction beneath central Peru. Part I: Crust and uppermost mantle: *J. Geophys. Res.*, **99**, 6899–6912.
- Jost, M. L. and R. B. Herrmann (1989), A student's guide to and review of moment tensors, *Earthquake Notes*, **60/2**, 37–57.
- Julian, B.R. and G.R. Foulger (1996), Earthquake mechanisms from linear-programming inversion of seismic-wave amplitude ratios, *Bull. Seism. Soc. Am.*, **86**, 972–980.
- Kennett, B. L. N., and E. R. Engdahl (1991), Traveltimes for global earthquake location and phase identification, *Geophys. J. Int.* **122**, 429–465. Source code for building the tables for both *iasp91* and *ak135*: **<http://www.iris.edu/pub/programs/iaspei-tau/>**.
- Kennett, B.L.N., E.R. Engdahl, and R. Buland (1995), Constraints on seismic velocities in the Earth from traveltimes. *Geophys. J. Int.*, **122**, 108–124.
- Kisslinger, C. (1980). Applications of  $S$  to  $P$  amplitude ratios for determining focal mechanisms from regional network observations, *Bull. Seism. Soc. Am.*, **70**, 999–1014.
- Kisslinger, C., J. R. Bowman, and K. Koch (1981). Procedures for computing focal mechanisms from local ( $SV/P$ ) ratios, *Bull. Seism. Soc. Am.*, **71**, 1718–1729. Correction for both this and the preceding paper was published in *BSSA* volume **72** on page 344.
- Kisslinger, C., J. R. Bowman, and K. Koch (1982). Determination of focal mechanisms from ( $SV/P$ ) amplitude ratios at small distances, *Phys. Earth and Planet. Inter.*, **30**, 172–176.

- Lahr, J. C. (1999), HYPOELLIPSE Y2K: A computer program for determining local earthquake hypocentral parameters, magnitude, and first-motion pattern, U.S. Geological Survey Open-file Report 99-023, 112p. On-line:  
<http://greenwood.cr.usgs.gov/pub/open-file-reports/ofr-99-0023>.  
[http://geohazards.cr.usgs.gov/iaspei\\_pgms/hypoellipse/](http://geohazards.cr.usgs.gov/iaspei_pgms/hypoellipse/) has the current version of the package, including documentation and executables for both PC and Sun/Unix.
- Malone, S. (1990), I.R.I.S. GOPHER UPDATE, *IRIS Newsletter*, **9** (4), 31–35,  
[https://www.iris.edu/hq/files/publications/iris\\_newsletters/doc/5.IRIS%20Newsletter-Vol.9Issue%204%20-%20Nov.%201990.pdf](https://www.iris.edu/hq/files/publications/iris_newsletters/doc/5.IRIS%20Newsletter-Vol.9Issue%204%20-%20Nov.%201990.pdf).
- Ottewill, L., P. Voss, J. Havskov (2016), SEISAN: EARTHQUAKE ANALYSIS SOFTWARE, <http://seis.geus.net/software/seisan/seisan.html>.
- Randall, G. R., C. J. Ammon and T. J. Owens (1995). Moment-tensor estimation using regional seismograms from a Tibetan Plateau portable network deployment, *Geophys. Res. Letters*, **22**, 1665–1668.
- Rau, R.-J., F.T. Wu, and T.-C. Shin (1996). Regional network focal mechanism determination using 3D velocity model and SH/P amplitude ratio, *Bull. Seism. Soc. Am.*, **86**, 1270–1283.
- Sipkin, S. A. (2001). USGS Moment tensor software and catalog, **International Handbook of Earthquake and Engineering Seismology** (W. H. K. Lee, H. Kanamori, P. C. Jennings, and C. Kisslinger, eds.), Academic Press, San Diego (Part B: 1629–1630 and accompanying CD).
- Snoke, J. A., J. W. Munsey, A. C. Teague, and G. A. Bollinger (1984), A program for focal mechanism determination by combined use of polarity and *SV-P* amplitude ratio data, *Earthquake Notes*, **55**, #3, 15.
- Snoke, J.A. (1989). Earthquake Mechanisms, **Encyclopedia of Geophysics** (D. E. James, Ed.), Van Nostrand Reinhold Company, New York, 239–245. A ODF copy: earth-mech89.pdf, is in the doc directory.
- Snoke, J.A. (1990), Clyde and the Gopher: a preliminary analysis of the 12 May 1990 Sakhalin Island event, Eastern Section of the SSA meeting (Blacksburg, VA, October), *Seism. Res. Letters*, **61**, 161.
- Snoke, J. A. (2003), FOCMEC: FOcal MEChanism determinations, **International Handbook of Earthquake and Engineering Seismology** (W. H. K. Lee, H. Kanamori, P. C. Jennings, and C. Kisslinger, eds.), Academic Press, San Diego (Part B: 1629–1630 and accompanying CD).
- Snoke, J.A. (2009), Traveltime Tables for iasp91 and ak135, *Seism. Res. Letters*, **80**(2), 260–262.

- Stein, S. and E. Klosko (2002), Earthquake Mechanisms and Plate Tectonics, **International Handbook of Earthquake and Engineering Seismology** (W. H. K. Lee, H. Kanamori, P. C. Jennings, and C. Kisslinger, Eds.), Academic Press, San Diego, Chapter 7.
- Wu, Q., M.C. Chapman, and J.N. Beale (2015), The Aftershock Sequence of the 2011 Mineral, Virginia Earthquake: Temporal and Spatial Distribution, Focal Mechanisms, Regional Stress and the Role of Coulomb Stress Transfer, *Bull. Seismol. Soc. Am.*, **105**, 2521–2537.

## Appendix A: Input conventions and format for *focmec*

This is a description of the input format for *focmec* (`./focmec/fmsub/focinp.f`).

**READ(1, '(A)') COMMT ! First line in input file**

**If there are N polarities or ratios in the data set, each one is read in in a single line. The file is terminated by an empty line.**

**MAX (in FOCMEC.INC) is the maximum number of allowed ratios plus polarities.**

**If the line is for a polarity, the program uses a read statement as follows:**

**READ(1, 5) STA, AZIN, TOANG1, SENSE**  
**5       FORMAT(A4, 2F8. 2, A1, F8. 4, 1X, A1, 1X, F6. 2, 1X, f6. 4, A)**

- STA is a name for the station. Up to four characters. Not used except as a label;
- AZIN is the azimuth (degrees) of the station measured from the epicenter. (North is 0° and East is 90°.);
- TOANG1 is the take-off angle (degrees) of the *S* or *P* polarity. The convention for the take-off angle is that 0° is down.;
- SENSE is a one-character key for a polarity or a ratio.

The *focmec* symbol conventions are:

**C = compression at station (plotted as a hexagon)**

**U = same as C (up on vertical)**

**D = dilatation --- down on vertical (plotted as a triangle)**

**+ = emergent compression (optionally included in focmec)**

**- = emergent dilatation (optionally included in focmec)**

**> = SH first motion to right (back to event, facing station) impulsive**

**< = SH first motion to left (back to event, facing station) impulsive**

**L = same as <**

**R = same as >**

**F = SV first motion away from event impulsive**

**B = SV first motion towards event impulsive**

**The SH and SV first motions are plotted as oriented arrows**

**l = SH first motion to left (back to event) emergent: optionally included**

**r = SH first motion to right (back to event) emergent: optionally included**

**b = SV first motion toward event emergent: optionally included**

**f = SV first motion away from event emergent: optionally included**

If one wants to have errors marked, follow the polarity with a duplicate line with an E in the symbol position. The error will then be flagged by a square superimposed on the polarity.

If the line is for a ratio, one uses the same format but there are more input parameters:

**5        READ(1, 5) STA, AZIN, TOANG1, SENSE, RATLOG, SNUMPOL, TOANG2, VPVS, INFO**  
**FORMAT(A4, 2F8. 2, A1, F8. 4, 1X, A1, 1X, F6. 2, 1X, f6. 4, A)**

SENSE is one of the following:

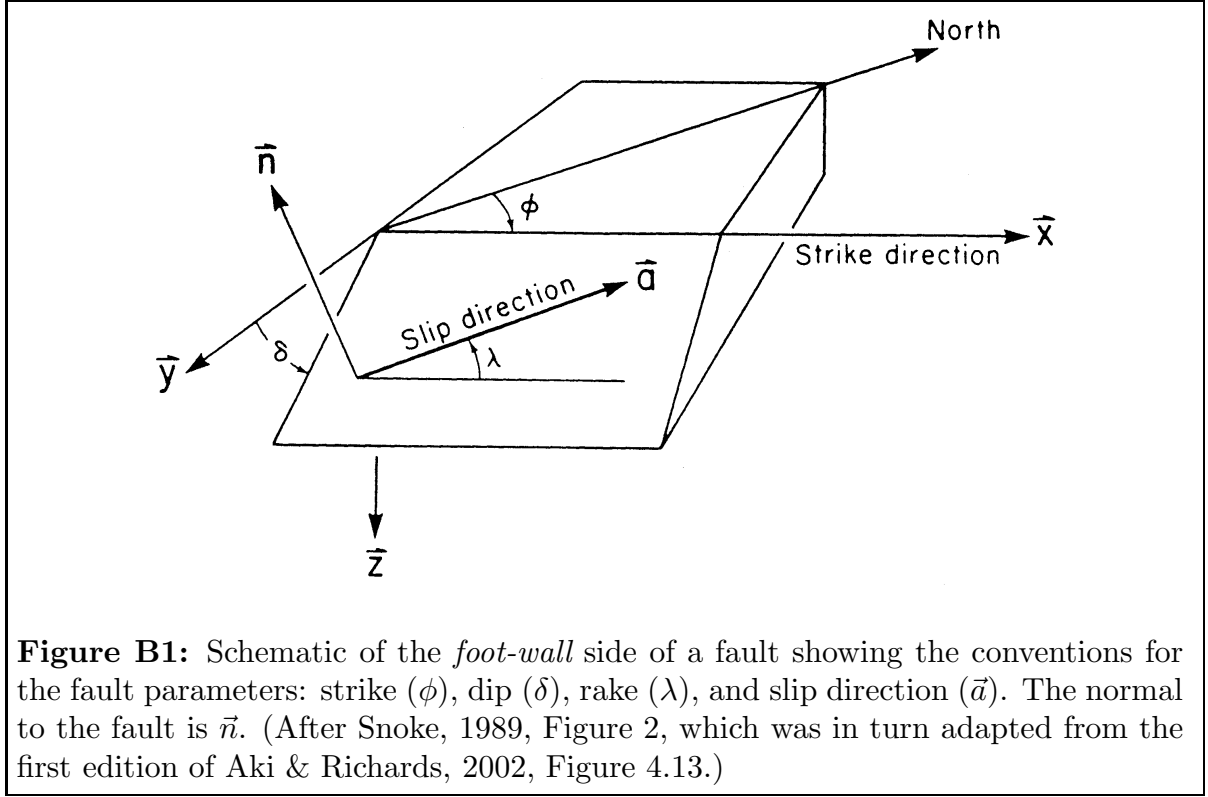
**H = Log10(SH/P)**  
**V = Log10(SV/P)**  
**S = Log10(SV/SH)**

Other input parameters:

- TOANG1 is the take-off angle of the  $S$ ;
- RATLOG is the  $\log_{10}$  of the ratio ( $S/P$  or  $SV/SH$ );
- SNUMPOL is the polarity of numerator  $S$ . It is not used, but is printed in the listing file along with the calculated values. Conventions used for the calculated polarities are L and R for  $SH$ , B and F for  $SV$ ;
- TOANG2 is the take-off angle of the phase in the denominator;
- VPVS is the  $v_P/v_S$  ratio at the source. In earlier versions of the *FOCMEC* package VPVS was not read in from the input file but entered as a prompt when running *focmec*. The change has been made because for a double-couple mechanism,  $(v_P/v_S)^3$  at the source is used to calculate the theoretical amplitude ratio so must be used in preparing the *focmec* input file. Input files written to run for pre-2017 versions of *focmec* need to run program *convert\_input* for each older input file. That program prompts for VPVS.;
- INFO is a field of up to 40 characters starting in column 46. If the input file was prepared by *focmec\_prep*, INFO summarizes information used in the amplitude ratio. (See *./focmec/sample\_runs/sakhalin* for an example.) There are only polarities in the input file in *./focmec/sample\_runs/ETNEvent*, but it has comments starting in column 40. For backward compatibility, *focmec* can handle such files and preserves the comments.

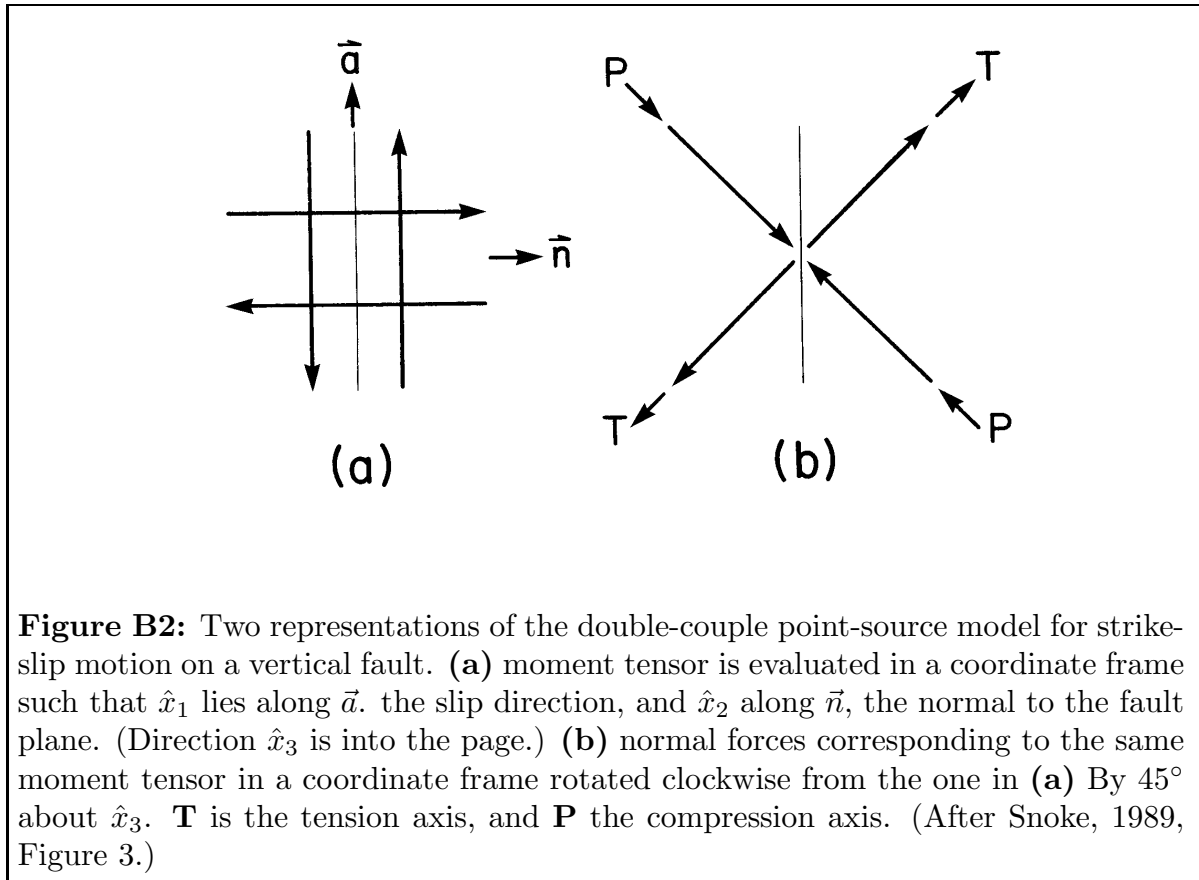
## Appendix B: Glossary for Focal Mechanisms

**Seismic Moment Tensor:** The ground displacement from an earthquake can be written as the convolution of a moment tensor and the gradient of a Green's function. The Green's function includes propagation effects, while the moment tensor contains information about the source properties. The moment tensor can be interpreted as the volume integral of the stress release associated with the earthquake. The most general moment tensor has six independent components, but the focal mechanisms for the vast majority of earthquakes are well described by a *double couple*, for which the moment tensor has only three independent components. See Jost & Herrmann (1989) for a comprehensive review of moment tensors.



**Strike, Dip and Rake:** One way to parameterize a double-couple solution is to specify, with three angles, the direction of a vector along the direction of slip of the earthquake along a fault surface. The **strike** ( $\phi$ ) is the azimuth of the fault, with the convention that if one faces down-dip, the strike direction is to the left. The **dip** ( $\delta$ ) is measured down from the horizontal and is bounded by  $0^\circ$  and  $90^\circ$ . The **rake** ( $\lambda$ ) is along the direction of slip on the fault surface and is bounded by  $-180^\circ$  and  $+180^\circ$ . The convention for rake angle  $\lambda$ : Reverse fault if  $0^\circ < \lambda < 180^\circ$ , normal fault if  $-180^\circ < \lambda < 0^\circ$ , right-lateral strike slip if  $\lambda = 180^\circ$ , and left-lateral strike slip if  $\lambda = 0^\circ$ . Note that with  $\hat{z}$  down (Figure B1), both  $(\hat{x}, \hat{y}, \hat{z})$  and (North, East,  $\hat{z}$ ) are right-handed coordinate frames.

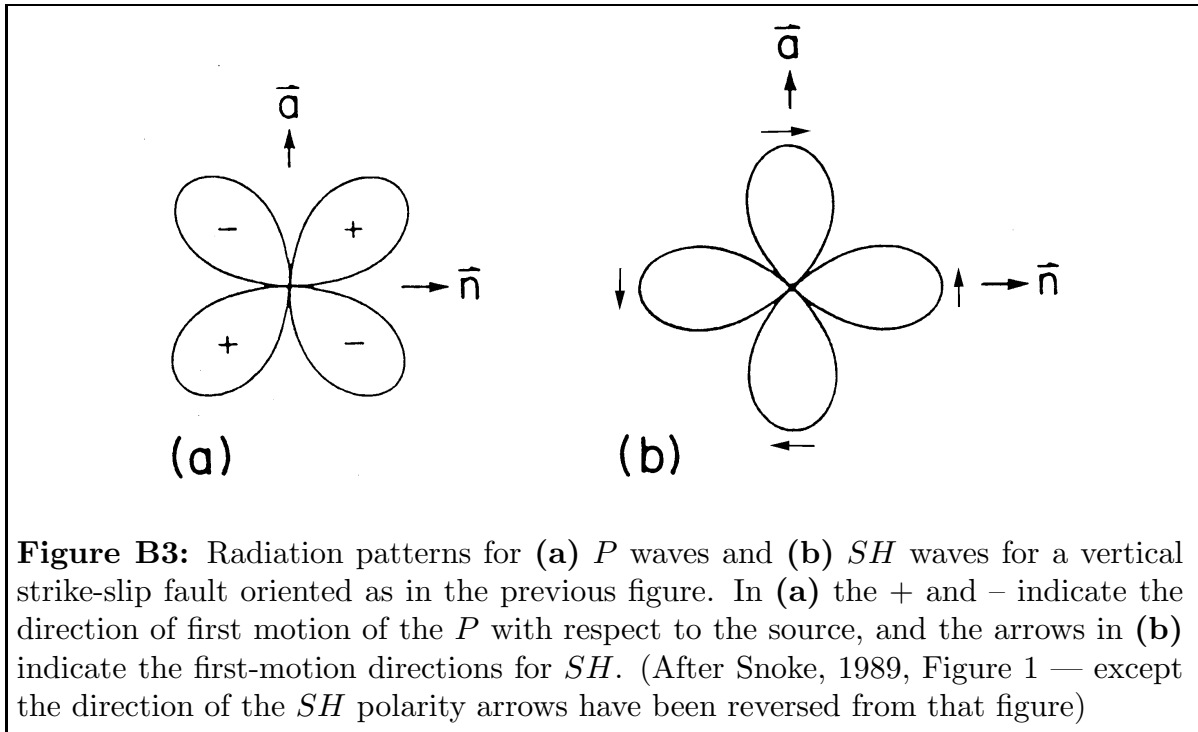
**Pressure and Tension Axes:** As shown in Figure B2, an alternative parameterization for a focal mechanism is to specify the trend and plunge of the **P** axis (direction of maximum source



**Focal Sphere:** Modeling the earthquake as a point source, the focal mechanism can be uniquely specified by specifying the directions of **P** and **T** with respect to a sphere of vanishingly small radius that surrounds the focus (Figure B2b). The **B** axis (or null axis) is along the intersection of the two fault planes — along  $\pm\hat{x}_3$  in Figure B2. Observations of polarities and amplitudes used to constrain the focal mechanism must be corrected to points on the focal sphere designated by the take-off angle and azimuth for the raypath from the source to that station. The particle motion is identical for antipodal points on the focal sphere, so a projection (from above) of station positions and focal mechanism onto the upper hemisphere can be mapped onto the lower hemisphere by simply adding  $180^\circ$  to all station azimuths and trends for the **P** and **T** axes. The projections of the focal spheres shown above in Figures 1 and 2 are lower-hemisphere projections. This is the more popular projection, presumably because most data are teleseismically recorded. Sometimes an upper-hemisphere projection is used, so it is instructive to review briefly how these projections are related and how one constructs them.

To make focal-mechanism plots, one projects the position on the focal sphere of the **P** and **T** axes (trends and plunges) and station polarities or amplitude ratios (take-off angles and azimuths) onto the focal sphere.

o thth (tsnbservatioioantn irities o746815745(f)3.87597(o)-32(c)2.3505(a)-1.874



**Radiation Pattern:** A double-couple solution produces a radiation pattern for  $P$  waves with four quadrants that are alternatively compressive and dilatational. Figure B3 shows the four quadrants for both the  $P$  and  $SH$  radiation patterns.

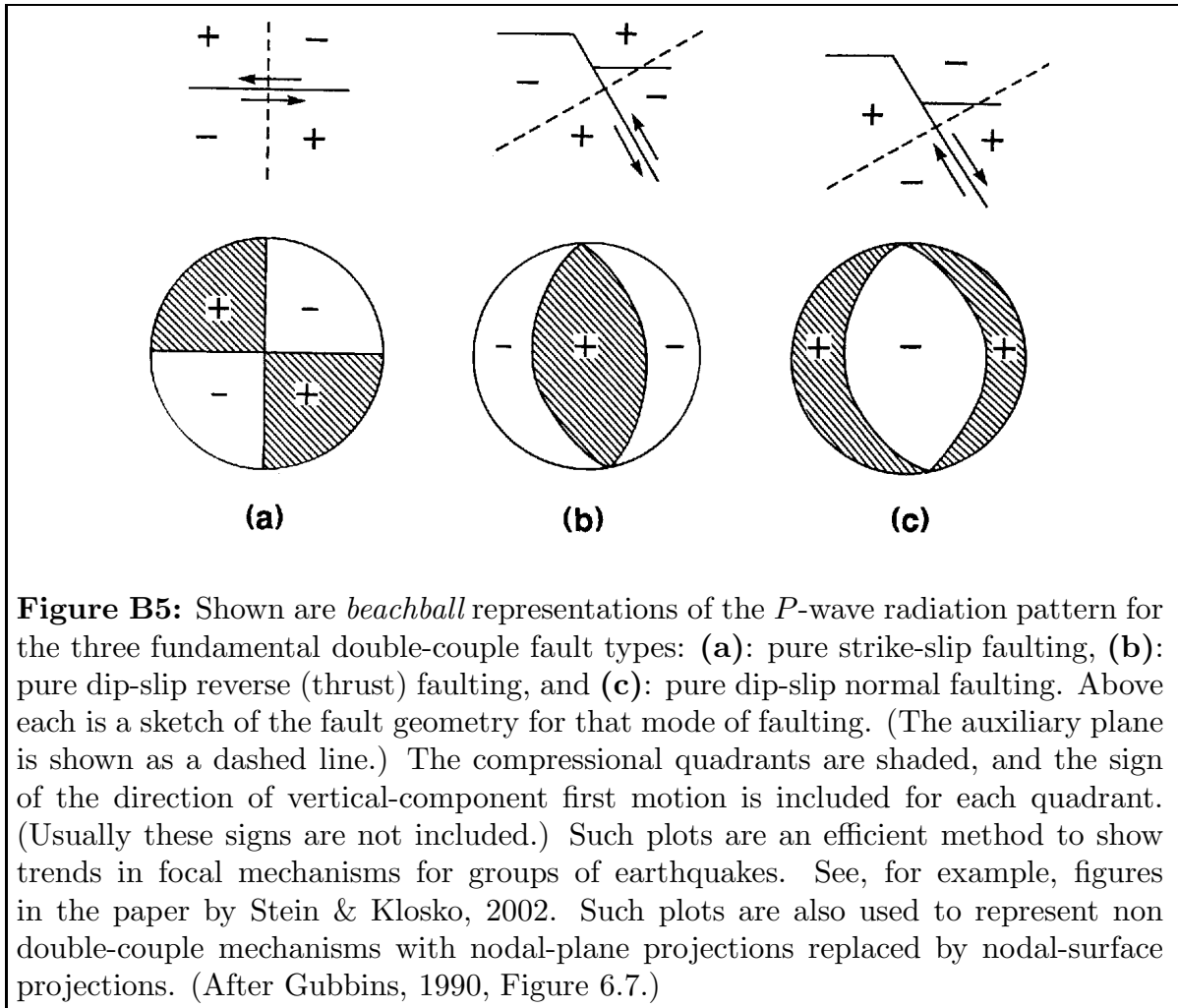
**Fault Plane and Auxiliary Fault Plane:** The radiation patterns for  $SV$  and  $SH$  have similar four-fold symmetry to that for  $P$ , and the result is that there are two equally possible fault planes consistent with all polarity and ratio data for a single “event” (point on the focal sphere). Hence for each solution, two possible sets of dip, strike and rake are presented, and each fault-plane plot includes two planes. Solutions produced by program *focmec* include the trend and plunge of vectors  $\mathbf{A}$  and  $\mathbf{N}$ , which are along the slip directions in the two possible fault planes ( $\vec{a}$  and  $\vec{n}$  in the preceding two figures in this section). These vectors can be gotten from  $\mathbf{P}$  and  $\mathbf{T}$  by a rotation of  $45^\circ$  around the vector  $\mathbf{B}$ , which is along the normal to the plane formed by  $\mathbf{P}$  and  $\mathbf{T}$ .

**Sign Conventions for Components of Ground Motion:** Polarities in the FOCMEC package are designated by directions with respect to an observer facing the station with his/her back to the epicenter. Accordingly,  $P$  arrival first motions are up or down,  $SH$  left or right, and  $SV$  forward or backward.

Horizontal components for a three-component seismograph must be rotated from *North-South* and *East-West* into *Radial* and *Transverse* to separate  $SV$  from  $SH$ . The convention in common usage — e.g., in SAC — has positive Radial as forward and positive Transverse as to the right with respect to an observer facing the station. Note that *Vertical*, *Radial*, and *Transverse* form a left-handed coordinate frame.



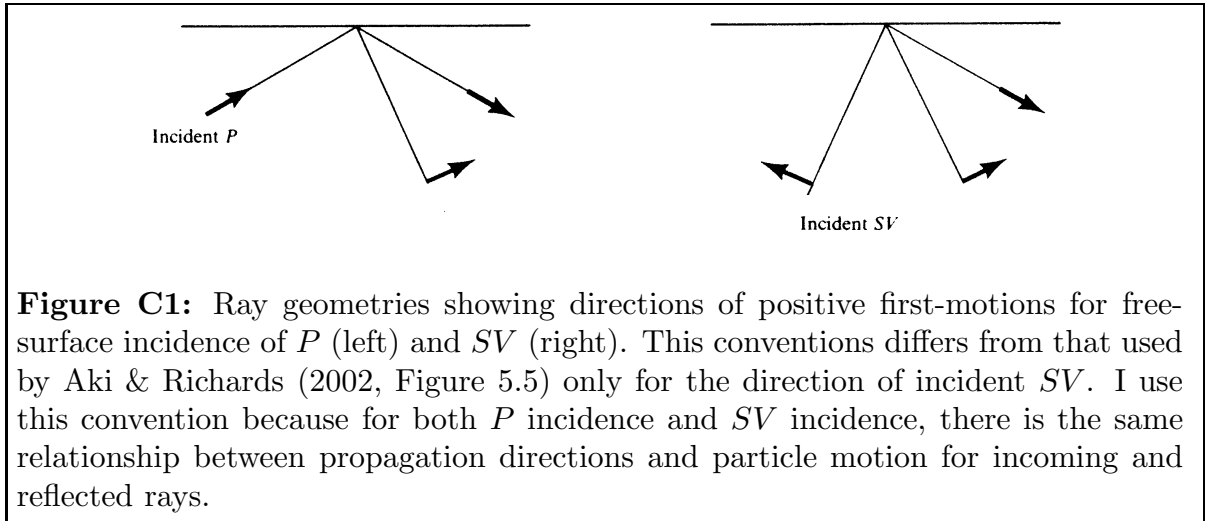


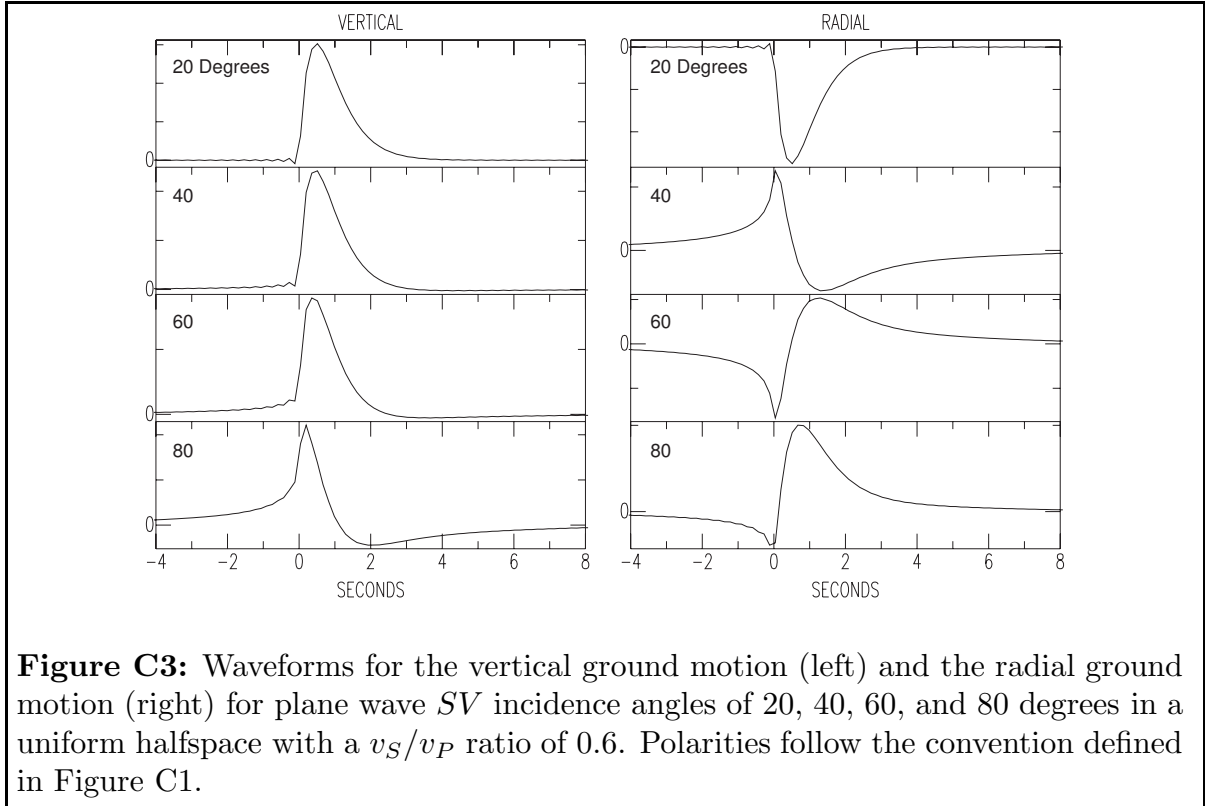
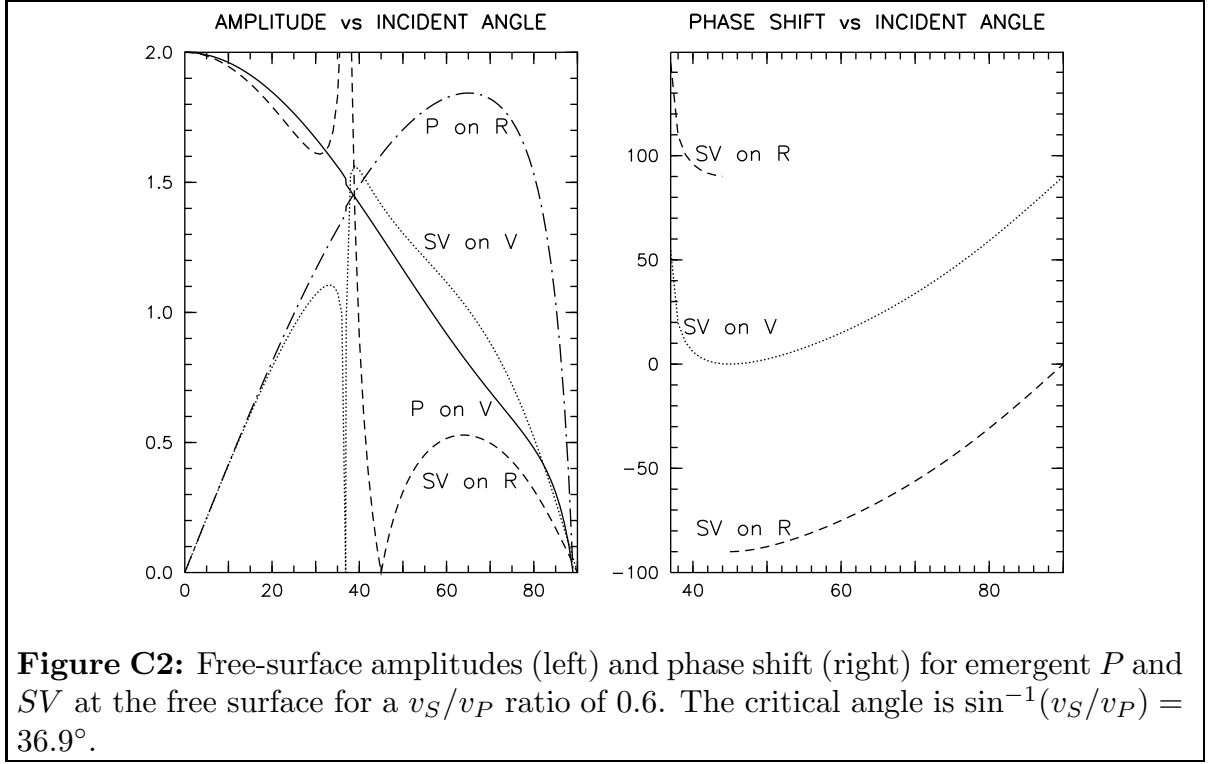


## Appendix C: *SV* Polarities and Amplitude Should be Used with Care

Kisslinger and coauthors (1980, 1981, 1982) describe procedures for using *SV/P* vertical-component amplitude ratios recorded by local and regional networks to constrain focal mechanisms. The emphasis was on the vertical components because at that time most networks used single-component seismographs and analog recording.

With modern instrumentation, one can often find well recorded *SV* arrivals — although generally not as well recorded as for the deep-focus Sakhalin Island event discussed above. We show below why *SV* should be used only with great care.





The input waveform for the ground motion shown in Figure C3 is normalized so that the area under the curve is the same as the amplitude for that component shown in Figure C2 when there is no phase shift. For  $P$  incidence, there is no critical angle and the polarities are all positive using the convention defined in Figure C1, so there is zero phase shift for all angles of incidence. The rest of this discussion is for  $SV$  incidence.

As discussed by Aki & Richards (2002, page 151), the sign of the “phase shift” depends on the Fourier sign convention and on the sign of the frequency. The phase shifts in Figure C2 use their conventions: positive frequencies and  $+i\omega t$  for the forward Fourier transform. Because of the different polarity for  $SV$  incidence between them and Figure C1, phase shifts presented here will differ by  $180^\circ$  from theirs.

Below critical angle incidence, the phase shift is zero for the vertical ground motion and  $180^\circ$  for the radial motion (see waveforms for  $20^\circ$  incidence in Figure C3). At  $45^\circ$  incidence, the phase shift for the radial component jumps by  $180^\circ$ , which can be seen in the polarity flip between the waveforms on the radial component for  $40^\circ$  and  $60^\circ$  in Figure C3.

The rapid changes in amplitude within a few degrees of the critical angle mean that neither the vertical nor radial component amplitudes should be used for arrivals at those angles.

One sees from Figure B4 above that for small emergence angles ( $22^\circ$  at COR for  $S$  for this event),  $SV$  is a sharp arrival on the radial but not on the vertical. In general, below about  $30^\circ$   $SV$  on the radial component is the more reliable.<sup>10</sup> For angles above the critical angle, the phase shift results in a drastic change in waveform for the radial component, so  $SV$  on the radial should definitely not be used in ratios and used only with great care for polarity.

For the vertical component with  $SV$  incidence, the polarity is stable up to about  $80^\circ$ , so those polarities can be used if the arrivals are well recorded. Up to about  $50^\circ$ , the small phase shift results in a negligible change in the amplitude, so the vertical component could be used in an amplitude ratio. At  $80^\circ$ , the waveform shown in Figure C3 is visibly changed and the amplitude is reduced to  $0.27/0.52 = 0.52$  the amplitude predicted by the free-surface correction plotted in Figure C2.

Kisslinger *et al.* (1961) wrote that the free-surface correction for the  $SV/P$  ratio on the vertical, the free-surface correction is close to unity for incidence angles from a few degrees above the critical angle to about  $80^\circ$ . While that is true based on the amplitudes shown in Figure C2 (see also their Figure 1), the effect of the phase shifts on the waveforms and amplitudes leads to a much larger variation for higher angles.

The above discussion is based on plane-wave incidence — appropriate for teleseismically recorded events. In their paper on shear-wave polarization, Booth & Crampin (1985) show that for curved wavefronts associated with local to near-regional events, an  $SP$  arrival that comes in just before direct  $S$  affects the observed waveforms. In addition, a low-velocity zone at the surface can complicate the waveforms — particularly for  $SV$  incidence. Such considerations must also be considered when choosing polarities and amplitudes for focal mechanism determinations.

---

<sup>10</sup>As seen in Figure 2,  $SV$  on the radial for KEV is still usable for a  $32^\circ$  emergence angle.

## Appendix D: Graphics in the *FOCMEC* package

Earlier versions of the *FOCMEC* package used the SAC (Goldstein, *et al.* 1998) Fortran library that was distributed with pre-1994 versions of SAC. That library allowed the user to create both plot files and interactive on-screen plots. The screen-plot option has been dropped, because the libraries became obsolete. Programs *focplt* and *ratplt* continues to use the SAC Graphics Format (SGF) to produce disk files. The self-contained program *sgftops* converts .sgf files to postscript (.ps) files. The *FOCMEC* package can be compiled and run on “big-endian” systems (Sun Solaris, Mac OSX PPC) or “little-endian” systems (Linux, Mac OSX i686/intel) that have the opposite byte order for binary data. As of 2014, program *sgftops* can handle either byte order.

Also included are four (Unix csh) scripts. These are all ASCII text files, so can be easily edited. All of these (except *plsgf*) require program *ghostscript* (often just called *gs*, which is available for all systems that can compile and run the *FOCMEC*-package programs.

1. *./focmec/bin/plsgf*: produces a print of a .sgf file.
2. *./focmec/bin/sgftoeeps*: produces a EPS file (Encapsulated Postscript file) from a .sgf file.
3. *./focmec/bin/sgftox* displays the input plot on the screen. As written, it calls *gs* to display the plot, but the script is easily edited to use other programs that display aEPS or PDF file.
4. *./focmec/bin/sgftopdf*: produces a PDF file from a .sgf file. Perl script *epstopdf* (<http://www.ctan.org/epstopdf>) is required.

To find out more about the program/ scripts, enter the name with no arguments.

The file *./focmec/doc/graphics.html* has more information about how to test the graphics package and how one can use the *symbol* routine to label plots.

Several scripts in Section 4 run program *focplt* to produce SGF files. Note that those for the Sakhalin Island event superimpose sets of data and solutions, so studying them may be helpful regarding how one answers the prompts. The screen output for these scripts is ported into a file named *a.junk* in the same directory, so if the script exits with an error message, comparing the contents of that file with the calling script should help the user find the error.

The scripts in *./focmec/sample\_runs* end with calls to *sgftopdf*, and the PDF plots are included in the *./focmec/doc* subdirectories for each application. The figures in this manual were produced from SGF plots using the script *sgftoeeps*.

## Appendix E The *focmec* Grid-Search Procedure

When *focmec* searches the focal sphere, it does it for a range of values for three angles: the trend and plunge of **B** (the null axis) and a range for “**Angle**”, which is the angle that **N** makes with the plane defined by the vertical (down) and the **B**-axis trend. (See Figures B2 and B3.) One is prompted for the minimum, increment, and maximum for each of these angles (in degrees). The default values will give an (approximately) equal-area search of the lower hemisphere of the focal sphere: 0° to 90° for the **B**-axis plunge with a 5° increment, 0° to 355° for the **B**-axis trend with a 5° increment, and 0° to 175° for **Angle** with a 5° increment.<sup>11</sup> For each solution that fits the selection criteria, the three angles are included in the output file *focmec.lst*.

In Section 4.2, I discuss and compare focal mechanisms for the Sakhalin Island event found using different data sets and different procedures to find the focal mechanism. In comparing the solutions, I wanted to see how well the 1990 NEIC/QED solution and the final CMT solution fit the data sets. Neither solution is found in the default *focmec* grid search.

Output from program *dsretc* includes the **B** trend and plunge, and as of 2017, **Angle**, so I ran it for the final CMT and the 1990 NEIC/QED focal mechanisms. I then hand-edited scripts that runs *focmec* to restrict the search accordingly. For example, the grid-search nine lines in the script *./focmec/sample\_events/sakhalin/rfocmec\_8staRW-cmtfixed* are

```

2. 29244E+02    B trend min
5. 00000E+00    B trend incr
2. 29244E+02    B trend max
2. 50855E+01    B plunge min
5. 00000E+00    B plunge incr
2. 50855E+01    B plune max
1. 05302E+02    Angle min
5. 00000E+00    Angle incr
1. 05302E+02    Angle max

```

Program *dsretc* can handle several kinds of input, and that was useful here. File *./focmec/doc/sakhalin-doc/CMT\_solution.pdf* reproduces the Web page for the final CMT solution. Included are angles for the two fault planes, the angles for the trend and plunge for the **P**, **T**, and **B** axes, and the six components of the moment tensor. All angles are given to the nearest degree, while the moment-tensor components are given to four significant figures. Using the moment-tensor input in program *dsretc*, all the angles in the output file are consistent with those on the final-CMT-solution page but have better precision.

---

<sup>11</sup>For the grid search, the **B**-axis plunge is the outer loop, and the search increment for the **B**-axis trend is divided by the cosine of the **B**-axis plunge.